Large Dynamic and Precision Optical Vector Analysis Assisted by SBS Processing

Min Xue, Qi Wang, Zongxin Xu, Yuqing Heng, Changyuan Yu, *Senior Member, IEEE*, and Shilong Pan, *Senior Member, IEEE*

***Abstract*—An optical vector analyzer assisted by stimulated Brillouin scattering (SBS) processing is proposed and experimentally demonstrated. Benefitting from the selective amplification and attenuation achieved by the SBS processing, the proposed OVA has enhanced dynamic range and measurement accuracy. An electro-optic modulator produces an intensity-modulated optical double-sideband (ODSB) signal. During the SBS processing, the +1st-order sideband of the ODSB signal is amplified while the -1st-order sideband is attenuated. Thus, an optical single-sideband signal owning a large sideband suppression ratio is achieved, which is then served as the probe signal and passes through an optical device-under-test. Then, by square-law detection, a photocurrent carrying the frequency responses is generated. Receiving and detecting the photocurrent, the multi-dimensional frequency responses, including magnitude, delay, and phase responses, are obtained. In an experiment, 34.05 dB amplification and 22.85 dB attenuation are achieved by the SBS processing. A dynamic range enhancement of 14.01 dB is obtained by measuring an optical bandpass filter, which is well coincident with the theoretical result. The comparative optical transfer delay measurement of a high-precision variable optical delay line indicates accuracy improvement.**

***Index Terms*—Delay measurement, microwave photonics, optical variable measurement, optical vector analysis, stimulated Brillouin scattering.**

I. Introduction

OPTICAL devices are now fundamental components and play an important role in emerging technologies and applications, such as microwave photonics radars [1], fifth-generation communication [2], high-precision optical sensing [3], and so on. Characterizing multi-dimensional frequency responses (e.g., magnitude, delay, phase, and polarization responses) is an indispensable process in their manufacture and the related innovations [4]–[7]. Hence, optical vector analysis techniques with the capability of multi-dimensional frequency responses have been proposed and implemented.

Conventionally, optical vector analysis is achieved based on the optical interferometry method [8]–[11], by which the only optical vector analyzer (OVA) on the market is implemented. The optical interferometer inherently has advantages of high measurement accuracy and large dynamic range but is very sensitive to environmental disturbance. Especially, optical device-under-tests (DUTs) should be connected in one arm of the optical interferometer. To achieve frequency responses measurement, ultrafast continuous wavelength scanning, together with temperature control and vibration isolation is necessary. Additionally, the coherence length of the laser source would place a limitation on the length of the DUT. To accurately characterize the optical devices with high fineness frequency structures, high-resolution OVAs using microwave photonics (MWP) techniques are proposed and constructed [12]–[17]. The key of the MWP-based OVAs is to use the MWP-based high-fineness optical frequency sweeping instead of the coarse all-optical wavelength sweeping. An attractive frequency resolution as high as 334 Hz was experimentally obtained [13]. The dynamic range and the measurement accuracy of the MWP-based OVA are obviously improved by innovative stimulated Brillouin scattering (SBS) processing [14]. However, limited by the bandwidth of electro-optic devices and microwave frequency sweeping range, the measurement range is small and extremely hard to extend. Another promising optical vector analysis is based on phase-shift (PS) techniques [18]–[22]. Compared with the two kinds of OVAs above, the PS-based OVA is of simple construction and cost-effective besides high stability and a large measurement range. Conventionally, to minimize the nonlinear measurement error, the electro-optic modulator works at a small modulation index. However, the dynamic range is also reduced, which is now a key restriction placed on the PS-based OVAs gaining ground.

In this paper, a PS-based OVA assisted by the SBS processing is proposed and implemented, which owns enhanced dynamic range and improved accuracy. In the proposed method, after the SBS processing, an optical single-sideband (OSSB) signal is achieved by amplifying the +1st-order sideband of an intensity-modulated (IM) optical double-sideband (ODSB) signal and attenuating the -1st-order sideband. Thanks to the selective amplification achieved by the SBS processing, the dynamic range is correspondingly enhanced. Furthermore, the sideband

Manuscript received September 25, 2021; revised November 29, 2021; accepted December 10, 2021. Date of publication December 17, 2021; date of current version April 18, 2022. This work was supported in part by the National Natural Science Foundation of China under Grant 62071226, in part by the National Key R&D Program of China under Grant 2017YFF0106900, and in part by HK RGC GRF under Grant 15209321. *(Corresponding author: Shilong Pan.)*

Min Xue, Qi Wang, Zongxin Xu, Yuqing Heng, and Shilong Pan are with the Key Laboratory of Radar Imaging and Microwave Photonics, Ministry of Education, Nanjing University of Aeronautics and Astronautics, Nanjing 210016, China (e-mail: xuemin@nuaa.edu.cn; wangqi_0207@nuaa.edu.cn; xu326578@nuaa.edu.cn; yuqingh@nuaa.edu.cn; pans@ieee.org).

Changyuan Yu is with the Department of Electronic and Information Engineering, The Hong Kong Polytechnic University, Hong Kong 999077, Hong Kong (e-mail: changyuan.yu@polyu.edu.hk).

Color versions of one or more figures in this article are available at https://doi.org/10.1109/JLT.2021.3135554.

Digital Object Identifier 10.1109/JLT.2021.3135554

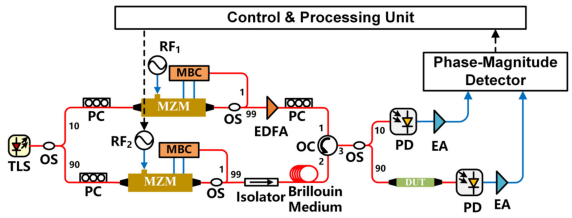

Fig. 1. Schematic diagram of the proposed OVA assisted by the SBS processing. TLS, tunable laser source; OS, optical splitter; MZM, Mach-Zehnder modulator; PC, polarization controller; EDFA, erbium-doped fiber amplifier; MBC, modulator bias controller; RF, radio frequency; OC, optical circulator; DUT, device under test; EA, electrical amplifier; PD, photodetector.

suppression ratio (SSR), presenting the power ratio of the +1st-order sideband to the undesired high-order sidebands induced by the nonlinear electrical-to-optical conversion, is dramatically enlarged. Thereby, the nonlinear measurement error is reduced. Experimentally, by the SBS processing, 34.05 dB amplification of the +1st-order sideband and 22.85 dB attenuation of the unwanted -1st-order sideband are achieved. Hence, the dynamic range improvement of 14.01 dB is observed by characterizing an optical bandpass filter (OBPF), which agrees well with the predicted improvement in theory. By comparing the measured optical transfer delays of a high-precision variable optical delay line, the improvement of the measurement accuracy is presented.

II. Analytical Analysis

Fig. 1 shows the schematic diagram of the PS-based OVA assisted by the SBS processing. An optical carrier signal is produced by a wavelength-swept tunable laser source (TLS). Then, an optical splitter separates the optical wavelength-swept signal into two portions. In the upper path, one portion is injected into a Mach-Zehnder modulator (MZM), wherein the optical signal is modulated by an RF signal with a frequency of f_{p}. Since the MZM works at the minimum transmission point (MITP), a carrier-suppressed ODSB signal is output. After amplification, the carrier-suppressed ODSB signal is used as a pumping signal. The other portion, in the lower path, is delivered to an MZM, which works at the quadrature transmission point (QTP). By applying an RF signal, an IM-ODSB signal is thus achieved. Mathematically, the electrical field can be described by

$$E_{\mathrm{IM}}(t)=\frac{\sqrt{2}}{2}E_{\mathrm{c}}\exp\left(i2\pi f_{\mathrm{c}}t\right)\left\{\exp\left[i\beta\sin\left(2\pi f_{\mathrm{e}}t\right)+i\frac{\pi}{2}\right]+\exp\left[i\beta\sin\left(2\pi f_{\mathrm{e}}t+\pi\right)\right]\right\} \tag{1}$$

where E_{c} and f_{c} are the amplitude and the frequency of the optical signal, respectively. f_{e} is the frequency of the RF signal and $\beta=\pi V/V_{\pi}$ is the MZM modulation index in the lower path wherein V_{π} is the half-wave voltage.

According to Jacobi-Anger expansion, the IM-ODSB signal is rewritten, given by

$$E_{\mathrm{IM}}(t)=\frac{\sqrt{2}}{2}E_{\mathrm{c}}\exp\left(i2\pi f_{\mathrm{c}}t\right)\times\sum_{m=-\infty}^{+\infty}J_m\left(\beta\right)\exp\left(im2\pi f_{\mathrm{e}}t\right)\left[i+(-1)^m\right] \tag{2}$$

where $J_m(\bullet)$ is the m-th order Bessel function of the first kind.

The IM-ODSB signal and the pumping signal are injected from two opposite directions of the Brillouin medium. To active the SBS, the frequency of the RF source in the upper path is carefully set, leading the RF frequency difference equal to the Brillouin frequency shift, e.g.,

$$f_{\mathrm{p}}-f_{\mathrm{e}}=f_{\mathrm{B}} \tag{3}$$

where f_{B} is the Brillouin frequency shift.

In the SBS processing, the +1st-order sideband is amplified and the -1st-order sideband is attenuated by the SBS gain and loss spectra, respectively. After the SBS processing, an OSSB signal is produced, which is

$$\begin{aligned}E_{\mathrm{SSB}}(t)&=H_{\mathrm{Gain}}\left(f_{\mathrm{c}}+f_{\mathrm{e}}\right)\times E_{\mathrm{c}}J_{+1}\left(\beta\right)\exp\left[i2\pi\left(f_{\mathrm{c}}+f_{\mathrm{e}}\right)t+i\frac{3\pi}{4}\right]\\&+E_{\mathrm{c}}J_0\left(\beta\right)\exp\left(i2\pi f_{\mathrm{c}}t+i\frac{\pi}{4}\right)\\&+H_{\mathrm{Loss}}\left(f_{\mathrm{c}}-f_{\mathrm{e}}\right)E_{\mathrm{c}}J_{+1}\left(\beta\right)\exp\left[i2\pi\left(f_{\mathrm{c}}-f_{\mathrm{e}}\right)t-i\frac{\pi}{4}\right]\\&+\frac{\sqrt{2}}{2}E_{\mathrm{c}}\exp(i2\pi f_{\mathrm{c}}t)\sum_{\substack{m=-\infty\\m\neq0,\pm1}}^{+\infty}J_m(\beta)\exp(im2\pi f_{\mathrm{e}}t)\left[i+(-1)^m\right]\end{aligned} \tag{4}$$

where $H_{\mathrm{Gain}}(f)$ and $H_{\mathrm{Loss}}(f)$ are the amplification and attenuation transmission functions of the SBS. At the right, the first term is the amplified +1st-order sideband while the third term is the attenuated -1st-order sideband. Typically, the amplification and attenuation beyond 20 dB are practically achievable. The fourth term is the high-order sidebands introduced by the nonlinear electrical-to-optical conversion. It is worth mentioning that the nonlinear error inherently exists, as the electrical-to-optical conversion is a nonlinear processing. Conventionally, the nonlinear measurement error is reduced by decreasing the modulation index. Thus, the suppressed -1st-order sideband as well as the high-order sidebands can be ignored. The SBS-processed optical signal can be simplified as

$$\begin{aligned}E_{\mathrm{SSB}}(t)&=H_{\mathrm{Gain}}\left(f_{\mathrm{c}}+f_{\mathrm{e}}\right)\times E_{\mathrm{c}}J_{+1}\left(\beta\right)\exp\left[i2\pi\left(f_{\mathrm{c}}+f_{\mathrm{e}}\right)t+i\frac{3\pi}{4}\right]\\&+E_{\mathrm{c}}J_0\left(\beta\right)\exp\left(i2\pi f_{\mathrm{c}}t+i\frac{\pi}{4}\right)\end{aligned} \tag{5}$$

After propagating through an optical DUT, the probe signal undergoes the amplitude and phase changes according to the transmission function, which is

$$\begin{aligned}E(t)&=H_{\mathrm{Gain}}\left(f_{\mathrm{c}}+f_{\mathrm{e}}\right)\times H(f_{\mathrm{c}}+f_{\mathrm{e}})E_{\mathrm{c}}J_{+1}(\beta)\exp\left[i2\pi\left(f_{\mathrm{c}}+f_{\mathrm{e}}\right)t+i\frac{3\pi}{4}\right]\\&+H\left(f_{\mathrm{c}}\right)E_{\mathrm{c}}J_0\left(\beta\right)\exp\left(i2\pi f_{\mathrm{c}}t+i\frac{\pi}{4}\right)\end{aligned} \tag{6}$$

where $H(f)=H_{\mathrm{sys}}(f)\bullet H_{\mathrm{DUT}}(f)$ is the joint transmission function. $H_{\mathrm{sys}}(f)$ and $H_{\mathrm{DUT}}(f)$ respectively present the system and the DUT transmission functions.

By square-law detection of a photodetector, the information of the joint frequency responses carried by the optical signal is transferred to the electrical domain. The desired f_e component in the generated photocurrent can be expressed as

$$i(f_e) = \eta H_{\text{Gain}}(f_c + f_e) \times H(f_c + f_e) H^*(f_c) E_c^2 J_{+1}(\beta) J_0(\beta) \exp\left(i\frac{\pi}{2}\right) \quad (7)$$

where η is related to the responsivity of the photodetector.

To de-embed the transmission function of the system and the amplification transmission function of the SBS, a through calibration processing is performed. Connecting the two test ports directly, where $H_{\text{DUT}}(f) = 1$, the desired component in the generated photocurrent is

$$i_{\text{sys}}(f_e) = \eta H_{\text{Gain}}(f_c + f_e) \times H_{\text{sys}}(f_c + f_e) H_{\text{sys}}^*(f_c) E_c^2 J_{+1}(\beta) J_0(\beta) \exp\left(i\frac{\pi}{2}\right) \quad (8)$$

Considering that the RF frequency is much smaller than the frequency sweep step of the TLS, it can be assumed that the magnitude responses are the same and the phase responses linearly change around the optical carrier. Hence,

$$|H_{\text{DUT}}(f_c + f_e)| = |H_{\text{DUT}}(f_c)| \quad (9)$$

$$\arg\left[H_{\text{DUT}}(f_c + f_e) H_{\text{DUT}}^*(f_c)\right] = \arg\left[H_{\text{DUT}}(f_c + f_e)\right] - \arg\left[H_{\text{DUT}}(f_c)\right] \quad (10)$$

where arg(•) gives the phase in radian.

In accordance with (7)–(9), the magnitude and delay responses can be given by

$$|H_{\text{DUT}}(f_c)| = \sqrt{\left|\frac{i(f_e)}{i_{\text{sys}}(f_e)}\right|} \quad (11)$$

$$\tau_{\text{DUT}}(f_c) = \frac{\arg\left[H_{\text{DUT}}(f_c + f_e)\right] - \arg\left[H_{\text{DUT}}(f_c)\right]}{2\pi f_e} = \arg\left[\frac{i(f_e)}{i_{\text{sys}}(f_e)}\right] \cdot \frac{1}{2\pi f_e} \quad (12)$$

The phase response is achieved by integrating the delay response, which is

$$\arg\left[H_{\text{DUT}}(f_c)\right] = \int_{f_s}^{f_c} \tau_{\text{DUT}}(f) \cdot 2\pi df \quad (13)$$

where f_s is the first frequency of the TLS. By scanning the frequency of the optical signal from the TLS, the frequency responses, including magnitude, delay, and phase responses, are measured.

It is worth noting, benefitting from the SBS amplification, an enlarged dynamic range is obtained. Considering the suppressed -1st-order sideband, the improvement of the dynamic range, compared with the traditional PS-based OVA, is given by

$$G(f_c) = \sqrt{\frac{|H_{\text{Gain}}(f_c + f_e)|}{2}} \quad (14)$$

Since the magnitude response is achieved by the square root detection in the PS-based OVA as shown in (11), the dynamic range improvement is lossy compared with the improvement in [14]. Moreover, only the desired +1st-order sideband undergoes the amplification, since the SBS amplification has excellent selectivity. It equivalently enlarges the power ratio of the desired +1st-order sideband to the undesired high-order sidebands. As a result, the nonlinear measurement error is suppressed considering beyond 20 dB amplification of the SBS processing.

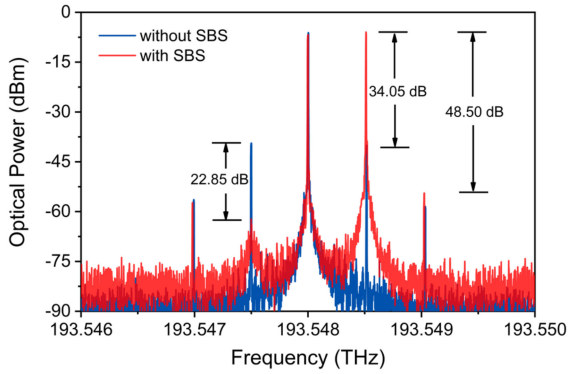

Fig. 2. The optical spectra of the IM-ODSB signal and the OSSB signal achieved by the SBS processing.

III. Experimental Results

An SBS-assisted PS-based OVA is constructed based on Fig. 1, by which an experiment is carried out. A high-power tunable laser (EXFO Inc. T100S-HP) provides a wavelength-swept optical signal with an optical power of 13 dBm, which is then divided by a 90/10 fiber splitter. In the upper path, the 10% output is delivered into an electro-optic MZM (Fujitsu FTM7938EZ), which is driven by a microwave signal generator (Keysight N5183B MXG). To active the SBS effect, an EDFA, manufactured by Amonics Inc., is cascaded to provide proper optical power amplification. The 90% output is delivered into an MZM biased at the QTP. Driven by a fixed microwave signal with an RF power of 0 dBm from a four-port vector network analyzer (VNA, R&S ZVA67), an IM-ODSB signal is generated. Two modulator bias controllers manufactured by YYLabs Inc. are employed to set the working point of the MZMs. An optical circulator is used to counter-propagate the signals of both branches. A 10.17-km single-mode fiber (SMF) is served as Brillouin medium. Two photodetectors (Finisar XPDV2120R) respectively convert the two optical signals into photocurrents, which are then amplified by electrical low noise amplifiers (RF Bay LNA-1450). The VNA synchronously receives the two photocurrents and extracts the differences of the magnitude and phase information. A WaveShaper 4000S Multiport Optical Processor, an optical tunable bandpass filter (Yenista XTM-50), and a motorized variable optical delay line (General Photonics MDL-002) are respectively served as the DUTs. A high-resolution optical spectrum analyzer (OSA, APEX AP2040C) with a frequency resolution up to 5 MHz is used to monitor the optical signals.

Fig. 2 shows the optical spectra of the IM-ODSB signal and the OSSB signal achieved by the SBS processing, when a 500 MHz RF signal is applied. The microwave signal in the upper path is fine-tuned to make the RF frequency difference be equal

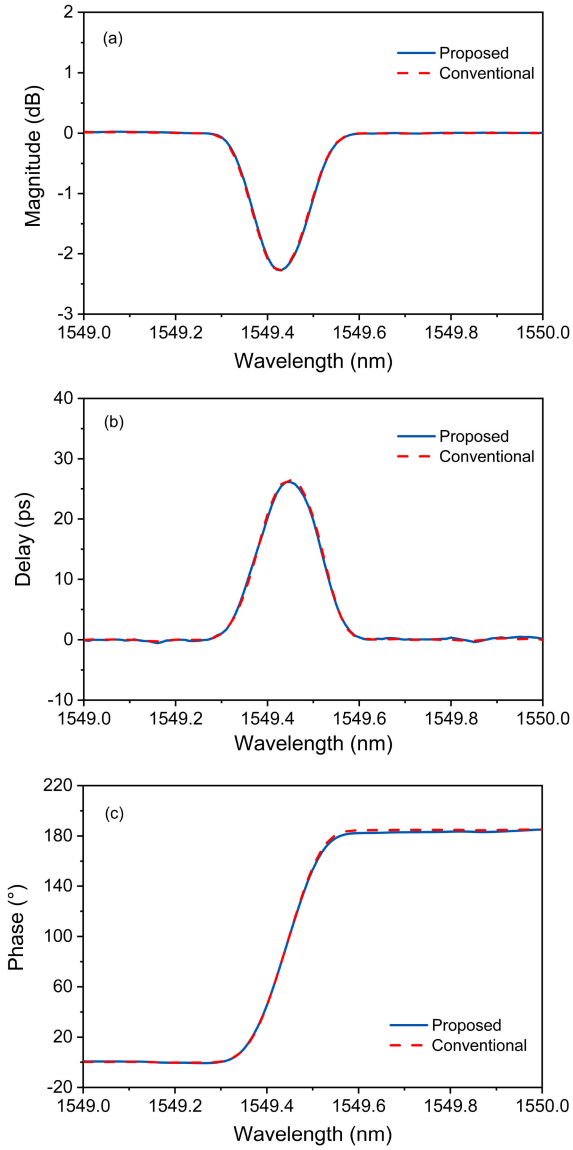

Fig. 3. The frequency responses of the programmable optical processor with Hilbert transformation measured by the conventional and the proposed OVAs. (a) The magnitude, (b) delay, and (c) phase responses.

to the Brillouin frequency shift of the 10.17-km SMF (e.g., 10.835 GHz @ 1550 nm). As can be seen, benefitting from the SBS processing, 34.05 dB amplification of the +1st-order sideband and 22.85 dB attenuation of the unwanted -1st-order sideband are obtained. According to (14), the 34.05 dB SBS amplification would bring a 14.025 dB dynamic range improvement in theory. Moreover, the selective amplification of the SBS enhances the SSR. The enhanced SSR is up to 48.50 dB. Hence, the residual nonlinear measurement error is only 1.07%, which is small enough to be ignored. It should be noted that the RF power should be properly set. By applying a small RF power, the nonlinear error is ignorable, but the dynamic range is small. A large RF power would bring a large dynamic range together with considerable nonlinear error.

Fig. 3 shows the measured frequency responses of the programmable optical processor with Hilbert transformation. As

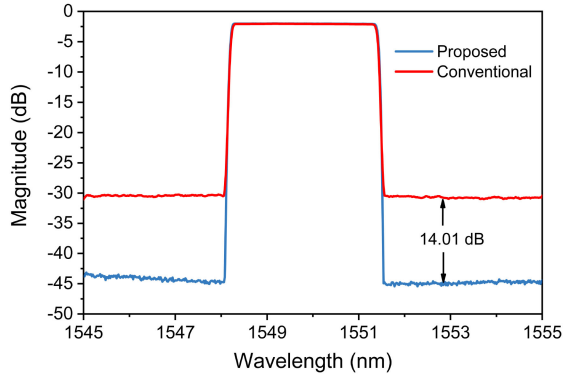

Fig. 4. The magnitude responses of the OBPF measured by the conventional and the proposed OVAs.

can be seen from Fig. 3(a) and (b), the magnitude and delay responses measured by the conventional PS-based OVA (red dash lines) are well coincident with those measured by the proposed SBS-assisted OVA (blue solid lines). Fig. (c) shows that the phase responses, achieved by respectively integrating the delay responses, also have a good coincidence. Moreover, the phase reversion of 180-degree around 1549.43 nm agrees well with the designed transfer response of an optical Hilbert transformer, verifying the high accuracy of the measurement system. It should be noted that, due to the small insertion loss of the optical Hilbert transformer (around 2.28 dB), the measured frequency responses cannot demonstrate the difference induced by the dynamic range.

To investigate the dynamic range enhancement benefitting from the SBS amplification, an OBPF with an out-of-band suppression larger than 40 dB is characterized by the conventional and the proposed OVA, respectively. Fig. 4 shows the measured magnitude responses of the OBPF. It is observed that, the measured magnitude responses within the insertion loss of 30 dB, including the passband and the partial rising & falling edges, are greatly overlapped, indicating a good coincidence. Limited by the small dynamic range of the conventional OVA, the measurable insertion loss is only 30.80 dB. Thanks to the selective amplification and attenuation of the SBS, the dynamic range of the proposed OVA is evidently enhanced. Hence, the larger insertion loss of 44.81 dB is achieved. A dynamic range enhancement of up to 14.01 dB is presented, which confirms the given dynamic range enlargement of 14.025 dB according to the SBS amplification in the experiment and analytical analysis.

It is worth mentioning that, to achieve maximum SBS amplification, the frequency of the RF signal in the upper path should be fine-tuned during the optical wavelength sweeping. It is because that the Brillouin frequency shift is optical wavelength-dependent. Fig. 5 shows the measured Brillouin frequency shifts at different wavelengths. As can be seen, the Brillouin frequency shift linearly decreases from 10.869 GHz to 10.801 GHz when the optical wavelength sweeps from 1545 nm to 1555 nm. By linear fitting, the change rate of the Brillouin frequency shift with the wavelength is observed, which is around 6.79 MHz/nm.

To present accuracy improvement, an experiment to measure the delays of a variable optical delay line is carried out. The

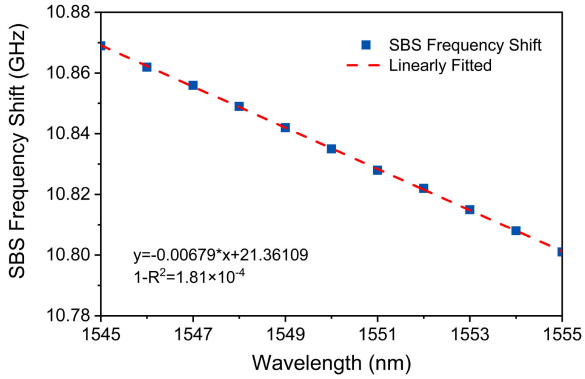

Fig. 5. The measured Brillouin frequency shifts at different wavelengths.

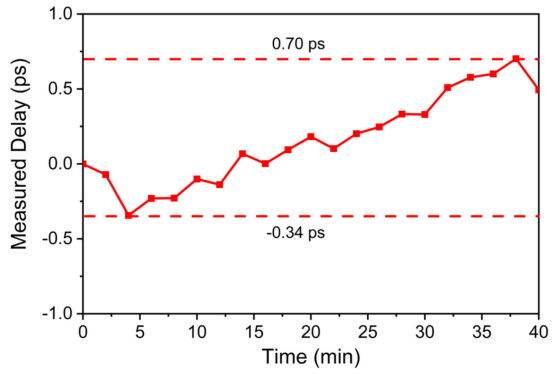

Fig. 7. The stability investigation of the proposed OVA in 40 minutes.

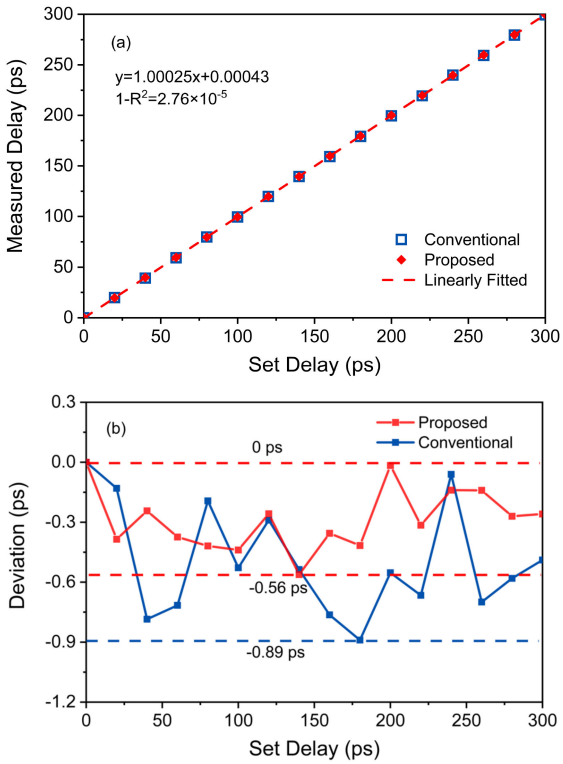

Fig. 6. The measured results of an optical delay line with different delays by the conventional and the proposed OVAs. (a) The optical transfer delays and (b) the deviations.

optical transfer delay of the variable optical delay line rises from 20 ps to 300 ps with an optical delay step of 20 ps. Fig. 6 shows the measured optical transfer delays at the set delays and the measurement errors by using the conventional and proposed OVAs. As shown in Fig. 6(a), the optical transfer delays measured by the proposed OVA (red solid diamonds) are exactly overlapped with those obtained by the traditional OVA (blue hollow squares). The measurement results are linearly fitted as shown the red dash line in Fig. 6(a). The R-square is up to 1, which indicates the high linearity and high measurement accuracy. To reveal the detailed measurement accuracy, Fig. 6(b) shows the deviations between the measured optical transfer delays and the set delays. The deviations achieved by the conventional OVA measurement results fluctuate within 0.89 ps, while the results achieved by the proposed OVA have a smaller deviation range of 0.56 ps. By comparison, an obvious accuracy improvement is obtained. The influence of the delay inaccuracy, induced by the variable optical delay line on the deviations, is ignorable since the delay inaccuracy is better than 10 fs, which is much smaller than the deviations. It should be noted, since the through calibration processing is performed when the delay is set to 0 ps, no measurement error appears in the measured magnitude responses. In this case, the generated photocurrents in the calibration and measurement processes are always the same. On the contrary, the rates of the phase responses are changed in accordance with the delays.

Fig. 7 shows the long-term stability, wherein the optical transfer delay is measured by per 2 minutes during 40 minutes after calibration. As can be seen, the measured delays unpredictably change between −0.34 ps and 0.70 ps, which are mainly caused by the room temperature fluctuation in the lab. The temperature fluctuation results in not only the length change of the fibers in the system but also the working point drifting of the MZM. It is believed that, by good temperature controlling, the stability can be further improved.

IV. Conclusion And Discussion

A PS-based OVA assisted by the SBS processing is proposed and experimentally demonstrated. Thanks to the selective SBS amplification, the dynamic range is evidently enhanced, and the nonlinear measurement error is suppressed. In the experiment, a programmable optical processor owning Hilbert transformation response, an optical bandpass filter, and a motorized variable optical delay line are precisely characterized. The measurement results confirm the dynamic range enhancement and the accuracy improvement given by analytical analysis. If a phase-modulated ODSB signal is employed, the measurement error induced by the bias point drifting can be eliminated and the measurement error can be further improved. Additionally, the delay measurement range can be significantly enlarged up to hundreds or even thoughts of times by finely sweeping the frequency of the RF source [23]. It is because the delay measurement range is determined by the 2π phase change and the angular frequency resolution.

REFERENCES

[1] S. Pan and Y. Zhang, "Microwave photonic radars," *IEEE J. Lightw. Tech.*, vol. 38, no. 19, pp. 5450–5484, Oct. 2020.

[2] V. A. Carey *et al.*, "Millimeter wave photonic tightly coupled array," *IEEE Trans. Antennas Propag.*, vol. 69, no. 8, pp. 4488–4503, Aug. 2021.

[3] A. Steinegger, O. S. Wolfbeis, and S. M. Borisov, "Optical sensing and imaging of pH values: Spectroscopies, materials, and applications," *Chem. Rev.*, vol. 120, no. 22, pp. 12357–12489, 2020.

[4] S. A. Miller *et al.*, "Large-scale optical phased array using a low-power multi-pass silicon photonic platform," *Optica*, vol. 7, no. 1, pp. 3–6, 2020.

[5] A. Boes, B. Corcoran, L. Chang, J. Bowers, and A. Mitchell, "Status and potential of lithium niobate on insulator (LNOI) for photonic integrated circuits," *Laser Photon. Rev.*, vol. 12, no. 4, pp. 1700256, 2018.

[6] M. Zhang *et al.*, "Broadband electro-optic frequency comb generation in a lithium niobate microring resonator," *Nature*, vol. 568, no. 7752, pp. 373–377, 2019.

[7] K. Zhong, X. Zhou, J. Huo, C. Yu, C. Lu, and A. P. T. Lau, "Digital signal processing for short-reach optical communications: A review of current technologies and future trends," *IEEE J. Lightw. Tech.*, vol. 36, no. 2, pp. 377–400, Jan. 2018.

[8] D. K. Gifford, B. J. Soller, M. S. Wolfe, and M. E. Froggatt, "Optical vector network analyzer for single-scan measurements of loss, group delay, and polarization mode dispersion," *Appl. Opt.*, vol. 44, no. 34, pp. 7282–7286, 2005.

[9] G. D. Vanwiggeren, A. R. Motamedi, and D. M. Barley, "Single-scan interferometric component analyzer," *IEEE Photon. Technol. Lett.*, vol. 15, no. 2, pp. 263–265, Feb. 2003.

[10] G. D. VanWiggeren and D. M. Baney, "Swept-wavelength interferometric analysis of multiport components," *IEEE Photon. Technol. Lett.*, vol. 15, no. 9, pp. 1267–1269, Sep. 2003.

[11] M. Volanthen, H. Geiger, M. J. Cole, R. I. Laming, and J. P. Dakin, "Low coherence technique to characterize reflectivity and time delay as a function of wavelength within a long fiber grating," *Electron. Lett.*, vol. 32, pp. 757–758, 1996.

[12] S. Pan and M. Xue, "Ultrahigh-resolution optical vector analysis based on optical single-sideband modulation," *IEEE J. Lightw. Tech.*, vol. 35, no. 4, pp. 836–845, Feb. 2017.

[13] T. Qing, S. P. Li, Z. Z. Tang, B. D. Gao, and S. L. Pan, "Optical vector analysis with attometer resolution, 90-dB dynamic range and THz bandwidth," *Nature Commun.*, vol. 10, pp. 5135, Nov. 2019.

[14] M. Sagues and A. Loayssa, "Swept optical single sideband modulation for spectral measurement applications using stimulated Brillouin scattering," *Opt. Exp.*, vol. 18, no. 16, pp. 17555–17568, 2010.

[15] J. Wen *et al.*, "Accuracy-enhanced wideband optical vector network analyzer based on double-sideband modulation," *IEEE J. Lightw. Technol.*, vol. 37, no. 13, pp. 2920–2926, Jul. 2019.

[16] W. Jun *et al.*, "Optical vector network analyzer based on double-sideband modulation," *Opt. Lett.*, vol. 42, no. 21, pp. 4426–4429, 2017.

[17] M. Wang and J. Yao, "Optical vector network analyzer based on unbalanced double-sideband modulation," *IEEE Photon. Technol. Lett.*, vol. 25, no. 8, pp. 753–756, Apr. 2013.

[18] T. Dennis and P. A. Williams, "Achieving high absolute accuracy for group-delay measurements using the modulation phase-shift technique," *IEEE J. Lightw. Technol.*, vol. 23, no. 11, pp. 3748–3754, Nov. 2005.

[19] G. Genty, T. Niemi, and H. Ludvigsen, "New method to improve the accuracy of group delay measurements using the phase-shift technique," *Opt. Commun.*, vol. 39, no. 12, pp. 119–126, 2002.

[20] W. Chen, M. Xue, D. Zhu, C. Yu, and S. Pan, "Optical vector analysis with improved accuracy and enhanced dynamic range," *IEEE Photon. Technol. Lett.*, vol. 31, no. 19, pp. 1565–1568, Oct. 2019.

[21] S. Ryu, Y. Horiuchi, and K. Mochizuki, "Novel chromatic dispersion measurement method over continuous gigahertz tuning range," *IEEE J. Lightw. Technol.*, vol. 7, no. 8, pp. 1177–1180, Aug. 1989.

[22] T. Niemi, M. Uusimaa, and H. Ludvigsen, "Limitations of phase-shift method in measuring dense group delay ripple of fiber Bragg gratings," *IEEE Photon. Technol. Lett.*, vol. 13, no. 12, pp. 1334–1336, Dec. 2001.

[23] S. P. Li *et al.*, "Optical fiber transfer delay measurement based on phase-derived ranging," *IEEE Photon. Technol. Lett.*, vol. 31, no. 16, pp. 1351–1354, Aug. 2019.

Min Xue received the B.S. and Ph.D. degrees in electronics engineering from the Nanjing University of Aeronautics and Astronautics, Nanjing, China, in 2011 and 2016, respectively. In 2016, he joined the College of Electronic and Information Engineering, Nanjing University of Aeronautics and Astronautics, where he is currently a Member of the Key Laboratory of Radar Imaging and Microwave Photonics, Ministry of Education. His research interests include photonic microwave measurement and metrology, optical fiber sensors, and integrated microwave photonics. He is the Publication Co-Chair of the IEEE International Topical Meeting on Microwave Photonics in 2017. Dr. Xue was the recipient of the Gold Medal with congratulations of the jury in the 45th International Exhibition of Inventions of Geneva in 2017 and the "Hong Kong Scholars" in 2018.

Qi Wang received the B.S. degree in electronics engineering in 2019 from the Nanjing University of Aeronautics and Astronautics, Nanjing, China, where she is currently working toward the M.S. degree.

Zongxin Xu is currently working toward the M.S. degree with the Key Laboratory of Radar Imaging and Microwave Photonics, Ministry of Education.

Yuqing Heng received the B.S. and M.S. degrees in electronics engineering from the Nanjing University of Aeronautics and Astronautics, Nanjing, China, in 2016 and 2019, respectively. She is currently working toward the Ph.D. degree.

Changyuan Yu (Senior Member, IEEE) received the Ph.D. degree in electrical engineering from the University of Southern California, Los Angeles, CA, USA, in 2005. In 2005, he was a Visiting Researcher with NEC Laboratories America, Princeton, NJ, USA. In December 2005, he joined as a Faculty with the National University of Singapore (NUS), Singapore, where he was the Founding Leader of the Photonic System Research Group, Department of Electrical and Computer Engineering. He was also a Joint Senior Scientist with the Institute for Infocomm Research (I^2R), Agency for Science, Technology and Research (A^*STAR), Singapore. In December 2015, he joined The Hong Kong Polytechnic University, Hong Kong, as a tenured Associate Professor with the Department of Electronic and Information Engineering. He also continues as an Adjunct Associate Professor with NUS. He has authored or coauthored six book chapters, and more than 400 journal articles and conference papers, which include 82 keynote/invited, including OFC2012 in USA. His research interests include photonic devices, subsystems, optical fiber communication and sensor systems, and biomedical instruments. His group won six best paper awards in conferences and the championship in biomedical area in the Third China Innovation and Entrepreneurship Competition in 2014.

Shilong Pan (Senior Member, IEEE) received the B.S. and Ph.D. degrees in electronic engineering from Tsinghua University, Beijing, China, in 2004 and 2008, respectively. From 2008 to 2010, he was a "Vision 2010" Postdoctoral Research Fellow with the Microwave Photonics Research Laboratory, University of Ottawa, Ottawa, ON, Canada. In 2010, he joined the College of Electronic and Information Engineering, Nanjing University of Aeronautics and Astronautics, Nanjing, China, where he is currently a Full Professor and an Executive Director of the Key Laboratory of Radar Imaging and Microwave Photonics, Ministry of Education. He has authored or coauthored more than 430 research articles, including more than 240 articles in peer-reviewed journals and 190 articles in conference proceedings. His research focuses on microwave photonics (MWP), which include optical generation and processing of microwave signals, photonic microwave measurement, and integrated MWP. Dr. Pan is a Fellow of OSA, SPIE, and IET. He was selected as an IEEE Photonics Society Distinguished Lecturer in 2019. He is currently an Associate Editor for the *Electronics Letters*, a Topical Editor of the *Chinese Optics Letters*, and a Technical Committee Member of the IEEE MTT-3 Microwave Photonics. He was the Chair for a number of international conferences, symposia, and workshops, the TPC Chair of the International Conference on Optical Communications and Networks in 2015, and the TPC Co-Chair for the IEEE International Topical Meeting on Microwave Photonics in 2017.